INTERNATIONAL JOURNAL FOR NUMERICAL METHODS IN ENGINEERING, VOL. 17, 679–706 (1981)

A UNIFORM STRAIN HEXAHEDRON AND QUADRILATERAL WITH ORTHOGONAL HOURGLASS CONTROL

D. P. FLANAGAN† AND T. BELYTSCHKO‡

Department of Civil Engineering, Northwestern University, Evanston, Illinois, U.S.A.

SUMMARY

The treatment of zero energy modes which arise due to one-point integration of first-order isoparametric finite elements is addressed. A method for precisely isolating these modes for arbitrary geometry is developed. Two hourglass control schemes, viscous and elastic, are presented and examined. In addition, a convenient one-point integration scheme which analytically integrates the element volume and uniform strain modes is presented.

INTRODUCTION

The 8-node three-dimensional and 4-node two-dimensional isoparametric elements are widely used in computational mechanics. Optimal integration schemes for these elements, however, present a difficult dilemma. Selective integration schemes, such as advanced by Malkus and Hughes,[1] provide good convergence for both compressible and nearly incompressible media by using a one-point integration for volumetric stresses and two-point quadrature in each direction for the deviatoric stresses. However, this involves four and eight additional evaluations of the equation of state for two- and three-dimensional problems, respectively. Thus, the use of selective schemes entails severe computational penalties for transient analysis.

However, the use of one-point quadrature schemes for both the volumetric and deviatoric stresses results in certain deformation modes remaining stressless. If a mesh is consistent with a global pattern of these (and perhaps rigid body) modes, they quickly dominate and destroy the solution. Such patterns are shown later in this paper. These modes are called kinematic, or zero energy, modes in the finite element literature, e.g. Irons and Ahmad,[2] and 'hourglass' modes for the hexahedron and quadrilateral in the finite difference literature. The term 'keystoning' has also been used by Key *et al.*[3]

Attempts to deal with this phenomenon appear first in finite difference literature where Maenchen and Sack[4] added artificial viscosity to inhibit opposing rotations of the sides. Such approaches were applied only in two-dimensional meshes. Furthermore, the hourglass viscosities were not independent of the uniform strain and rigid body modes of the element, which could degrade the solution.

Little thought was given in the finite difference literature as to the origin of these modes. It was first perceived by Petschek and Hanson[5] that the absence of bilinear terms in the velocity field accounts for the hourglass modes. This was also established in a finite element context by Belytschko.[6]

† Research Assistant.
‡ Professor of Civil Engineering.

0029–5981/81/050679–28$02.80

Received 26 August 1980

Wilkins *et al.*[7] developed a 'triangular' hourglass viscosity for the hexahedron. This technique is quite complex, involves considerable coding and computation, and is not independent of the deformation and rigid body modes. A finite element version of the Maenchen and Sack[4] anti-hourglass viscosity has been developed by Belytschko and Kennedy.[8]

The first to pursue the orthogonality of the hourglass modes to the first-order modes were Key[9] and Kosloff and Frazier.[10] Kosloff and Frazier also identified the similarity between their hourglass control and the incompatible element of Wilson *et al.*[11] which was introduced by the latter in finite element quadrilaterals to enhance their convergence in beam bending problems. However, adaption of their technique to non-rectilinear elements requires the solution of two sets of four simultaneous equations for the quadrilateral and four sets of eight equations for the hexahedron. Furthermore, this would be required for each element during each time step within a transient analysis code.

In this paper, a technique for precisely isolating the orthogonal hourglass mode shapes for both quadrilaterals and hexahedrons of arbitrary geometry is developed. In conjunction with this, a scheme which analytically integrates the hexahedral volume, without recourse to averaging schemes such as used by Wilkins *et al.*,[7] and the uniform strain modes is presented. The resulting algorithm is simple and elegant; only 20–30 FORTRAN statements are needed for both the evaluation of the internal and anti-hourglass nodal forces.

Numerical experiments are presented with both elastic and viscous resistance in the hourglass modes. A good check problem, the response of a beam to a uniform load, has been identified. Without hourglass control, the solution for certain boundary conditions quickly degenerates. It is shown that viscous resistance cannot completely stabilize the hourglass pattern, but elastic resistance works very well for even rather low stiffness parameters.

The majority of this paper is devoted to the hexahedron element. In a later section, we derive the method specific to the quadrilateral. Our integration procedure is equivalent to one-point quadrature for this element since the latter technique correctly assesses the volume of a quadrilateral. Still, our anti-hourglass technique is unique in its ability to utilize quantities already computed for integration of the uniform strain modes.

The methods are developed with regards to large deflections of isotropic, hypo-elastic (incrementally Hookean) materials. A Lagrangian mesh is assumed and Eulerian descriptions of kinematics and kinetics are employed throughout this paper.

KINEMATICS

The hexahedron element relates the spatial co-ordinates x_i to the nodal co-ordinates x_{iI} through the isoparametric shape functions ϕ_I as follows:

$$x_i = x_{iI}\phi_I(\xi, \eta, \zeta) \tag{1}$$

In accordance with indicial notation convention, repeated subscripts imply summation over the range of that subscript. The lowercase subscripts have a range of three, representing the spatial co-ordinate directions. Uppercase subscripts have a range of eight, corresponding to the element nodes.

The same shape functions are used to define the element displacement field in terms of the nodal displacements u_{iI}:

$$u_i = u_{iI}\phi_I \tag{2}$$

Since these shape functions apply to both spatial co-ordinates and displacements, their material derivative (represented by a superposed dot) must vanish. Hence, the velocity field may be given by

$$\dot{u}_i = \dot{u}_{iI}\phi_I \tag{3}$$

The velocity gradient $\dot{u}_{i,j}$ is defined as shown below. The deformation rate (velocity strain) tensor D_{ij} and vorticity (instantaneous rotation) tensor W_{ij} are the symmetric and anti-symmetric parts of the velocity gradient, respectively:

$$\dot{u}_{i,j} = \dot{u}_{iI}\phi_{I,j} \tag{4}$$

$$D_{ij} = \tfrac{1}{2}(\dot{u}_{i,j} + \dot{u}_{j,i}) \tag{5}$$

$$W_{ij} = \tfrac{1}{2}(\dot{u}_{i,j} - \dot{u}_{j,i}) \tag{6}$$

By convention, a comma preceding a lowercase subscript denotes differentiation with respect to the spatial co-ordinates, e.g. $\dot{u}_{i,j}$ denotes $\partial\dot{u}_i/\partial x_j$.

The isoparametric shape functions map a unit cube in ξ_i-space (ξ_i is denoted explicitly as (ξ, η, ζ)) to a general hexahedron in x_i-space. We choose to centre the unit cube at the origin in ξ_i-space so that the shape functions may be conveniently expanded in terms of an orthogonal set of base vectors, given in Table I, as follows:

$$\phi_I = \tfrac{1}{8}\Sigma_I + \tfrac{1}{4}\xi\Lambda_{1I} + \tfrac{1}{4}\eta\Lambda_{2I} + \tfrac{1}{4}\zeta\Lambda_{3I} + \tfrac{1}{2}\eta\zeta\Gamma_{1I} + \tfrac{1}{2}\zeta\xi\Gamma_{2I} + \tfrac{1}{2}\xi\eta\Gamma_{3I} + \xi\eta\zeta\Gamma_{4I} \tag{7}$$

Table I

Node	ξ	η	ζ	Σ_I	Λ_{1I}	Λ_{2I}	Λ_{3I}	Γ_{1I}	Γ_{2I}	Γ_{3I}	Γ_{4I}
1	$-\frac{1}{2}$	$-\frac{1}{2}$	$-\frac{1}{2}$	1	−1	−1	−1	1	1	1	−1
2	$\frac{1}{2}$	$-\frac{1}{2}$	$-\frac{1}{2}$	1	1	−1	−1	1	−1	−1	1
3	$\frac{1}{2}$	$\frac{1}{2}$	$-\frac{1}{2}$	1	1	1	−1	−1	−1	1	−1
4	$-\frac{1}{2}$	$\frac{1}{2}$	$-\frac{1}{2}$	1	−1	1	−1	−1	1	−1	1
5	$-\frac{1}{2}$	$-\frac{1}{2}$	$\frac{1}{2}$	1	−1	−1	1	−1	−1	1	1
6	$\frac{1}{2}$	$-\frac{1}{2}$	$\frac{1}{2}$	1	1	−1	1	−1	1	−1	−1
7	$\frac{1}{2}$	$\frac{1}{2}$	$\frac{1}{2}$	1	1	1	1	1	1	1	1
8	$-\frac{1}{2}$	$\frac{1}{2}$	$\frac{1}{2}$	1	−1	1	1	1	−1	−1	−1

The above vectors represent the displacement modes of a unit cube. The first vector, Σ_I, accounts for rigid body translation. We call Σ_I the summation vector since it may be employed in indicial notation to represent the algebraic sum of a vector.

The linear base vectors Λ_{iI} may be readily combined to define three uniform normal strain modes, three uniform shear strain modes and three rigid body rotation modes for the unit cube. We refer to Λ_{iI} as the volumetric base vectors since, as we will illustrate in the next section, they are the only base vectors which appear in the element volume expression.

The last four vectors $\Gamma_{\alpha I}$ (note that Greek subscripts have a range of four) give rise to linear strain modes which are neglected by one-point integration. These vectors define the hourglass patterns for a unit cube. Hence, we refer to $\Gamma_{\alpha I}$ as the hourglass base vectors.

ONE-POINT INTEGRATION

The principle of virtual work gives us the following relationship for the element nodal forces f_{iI}:

$$\dot{u}_{iI} f_{iI} = \int_V T_{ij} D_{ij} \, \mathrm{d}V \tag{8}$$

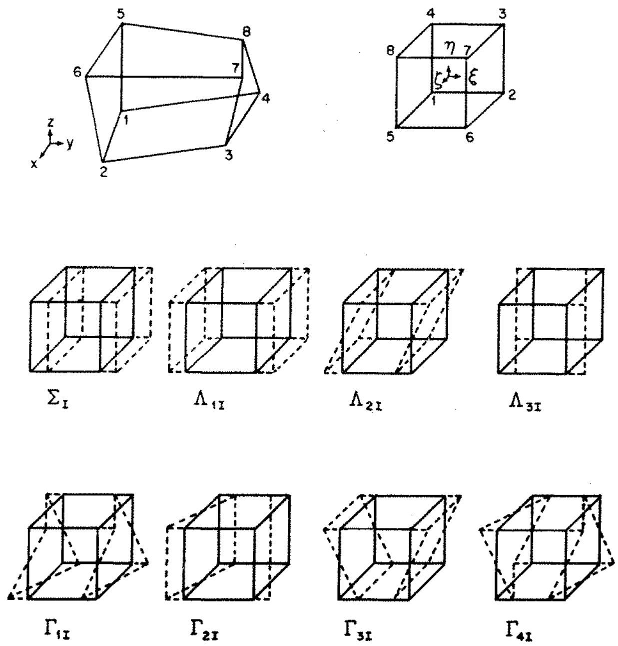

Figure 1. Hexahedron and its displacement modes; hourglass modes $\Gamma_{\alpha I}$

Since Cauchy's stress tensor T_{ij} (physical stress) is symmetric, the velocity gradient may replace the deformation rate tensor, D_{ij}, above.

We perform one-point integration by neglecting the nonlinear portion of the element displacement field, thereby considering a state of uniform strain and stress. The preceding expression is approximated by

$$\dot{u}_{iI} f_{iI} = V \bar{T}_{ij} \bar{\dot{u}}_{i,j} \tag{9}$$

$\bar{T}_{ij}$ represents the assumed uniform stress field and will be referred to as the mean stress tensor. By neglecting nonlinear displacements, we have assumed that the mean stresses depend only on the mean strains. Mean kinematic quantities are defined by integrating over the element as follows:

$$\bar{\dot{u}}_{i,j} = \frac{1}{V} \int_V \dot{u}_{i,j} \, \mathrm{d}V \tag{10}$$

We now define the B-matrix as

$$B_{iI} = \int_V \phi_{I,i} \, \mathrm{d}V \tag{11}$$

The mean velocity gradient, applying equation (4), is then given by

$$\bar{\dot{u}}_{i,j} = \frac{1}{V} \dot{u}_{iI} B_{jI} \tag{12}$$

Therefore, we may express the nodal forces by

$$f_{iI} = \bar{T}_{ij} B_{jI} \tag{13}$$

Computing nodal forces by this integration scheme requires evaluation of the B-matrix and volume. These two tasks are linked since

$$x_{i,j} = \delta_{ij} \tag{14}$$

Therefore, equations (11) and (1) yield

$$x_{iI} B_{jI} = \int_V (x_{iI} \phi_I)_{,j} \, \mathrm{d}V = V \delta_{ij} \tag{15}$$

Consequently, the B-matrix may alternatively be expressed by

$$B_{iI} = \frac{\partial V}{\partial x_{iI}} \tag{16}$$

To integrate the element volume in closed form, we use the Jacobian of the isoparametric transformation to transform to an integral over the unit cube:

$$V = \int_V \mathrm{d}V = \int_{-1/2}^{1/2} \int_{-1/2}^{1/2} \int_{-1/2}^{1/2} J \, \mathrm{d}\zeta \, \mathrm{d}\eta \, \mathrm{d}\xi \tag{17}$$

The Jacobian J is the determinant of the transformation operator $\partial x_i / \partial \xi_j$ and may be expressed as

$$J = e_{ijk} \frac{\partial x}{\partial \xi_i} \frac{\partial y}{\partial \xi_j} \frac{\partial z}{\partial \xi_k} \tag{18}$$

Note that the lowercase subscript notation for the spatial co-ordinates has been dropped here in favour of the explicit form (x, y, z). Using equations (1), (17) and (18), the element volume may be expressed in the following form:

$$V = x_I y_J z_K C_{IJK} \tag{19}$$

where

$$C_{IJK} = e_{ijk} \int_{-1/2}^{1/2} \int_{-1/2}^{1/2} \int_{-1/2}^{1/2} \frac{\partial \phi_I}{\partial \xi_i} \frac{\partial \phi_J}{\partial \xi_j} \frac{\partial \phi_K}{\partial \xi_k} \mathrm{d}\zeta \, \mathrm{d}\eta \, \mathrm{d}\xi \tag{20}$$

Observe that the coefficient array C_{IJK} is identical for all hexahedrons. Furthermore, it possesses the alternator properties, as given below:

$$C_{IJK} = C_{JKI} = C_{KIJ} = -C_{IKJ} = -C_{JIK} = -C_{KJI} \tag{21}$$

Therefore, applying equations (16) and (21) to the expression (19) yields the following form for evaluating the B-matrix:

$$B_{iI} = \begin{bmatrix} y_J z_K \\ z_J x_K \\ x_J y_K \end{bmatrix} C_{IJK} \tag{22}$$

Looking at the form of equation (7), it is evident that evaluating each component of C_{IJK} involves integrating a polynomial which is at most bi-quadratic. However, since we are integrating over a symmetric region, any term with a linear dependence will vanish. the only terms which survive the integration will be the constant, square, double square and triple square terms. Furthermore, the alternator properties cause half of these remaining terms to drop out.

The resulting expression for C_{IJK} is

$$C_{IJK} = \tfrac{1}{192} e_{ijk}(3\Lambda_{iI}\Lambda_{jJ}\Lambda_{kK} + \Lambda_{iI}\Gamma_{kJ}\Gamma_{jk} + \Gamma_{kI}\Lambda_{jJ}\Gamma_{iK} + \Gamma_{jI}\Gamma_{iJ}\Lambda_{kK}) \tag{23}$$

The above expression is evaluated using Table I, after which practical formulae for computing the B-matrix and volume are developed. These formulae appear in Appendix I.

The orthogonality of the base vectors in Table I and equation (23) indicate that Σ_I and $\Gamma_{\alpha I}$ are orthogonal to C_{IJK}:

$$C_{IJK}\Sigma_I = 0 \tag{24}$$

$$C_{IJK}\Gamma_{\alpha I} = 0 \tag{25}$$

Furthermore, equation (22) implies that Σ_I and $\Gamma_{\alpha I}$ are also orthogonal to B_{iI}.

$$B_{iI}\Sigma_I = 0 \tag{26}$$

$$B_{iI}\Gamma_{\alpha I} = 0 \tag{27}$$

The conditions (24) and (25) and equation (19) prove our earlier assertion that only the volumetric base vectors, Λ_{iI}, account for element volume. Similarly, equations (26) and (27) imply that the B-matrix contains only components of the volumetric base vectors. Therefore, by equation (12) and (13), only these base vectors lead to stresses or nodal forces within the one-point integration framework.

It is worth noting at this point the difference between the mean stress approach and one-point quadrature. The latter method would effectively neglect the last three terms of equation (23). In a parallelepiped, the nodal co-ordinates contain no component of the hourglass base vectors and, consequently, only the first term of equation (23) is necessary to compute the B-matrix and volume. In such a case, one-point quadrature is equivalent to the mean stress formula. However, for a general hexahedron, one-point quadrature does not correctly assess a state of uniform stress and strain, and may not be convergent (see Zienkiewicz).[12]

STRESS–STRAIN RELATIONSHIPS

The integration scheme we have just described does not assume any constitutive law, i.e. it is material independent. The only stipulation is that the stress state does not depend on the nonlinear portion of the element displacement field. Hence, the mean stresses must be related only to the mean strain rates (as opposed to the full strain field) through the governing material law.

To illustrate this procedure, we will assume an isotropic, hypo-elastic material. The physical stress rate for such a material, in terms of mean quantities, is given by

$$\dot{\bar{T}}_{ij} = \bar{T}^{\nabla}_{ij} + \bar{W}_{ik}\bar{T}_{kj} + \bar{W}_{jk}\bar{T}_{ki} \tag{28}$$

where $\bar{T}^{\nabla}_{ij}$ is the Jaumman rate which, for this material, obeys Hooke's law:

$$\bar{T}^{\nabla}_{ij} = \lambda\bar{D}_{kk}\delta_{ij} + 2\mu\bar{D}_{ij} \tag{29}$$

The mean deformation rate tensor $\bar{D}_{ij}$ and vorticity tensor $\bar{W}_{ij}$ are defined in terms of the mean velocity gradient (12) through equations (5) and (6), respectively. The Lamé coefficients λ and μ need not be constant.

Assuming the preceding constitutive law, we can develop natural response modes, or eigenmodes, for the hexahedron. This analysis is useful in establishing the stability limit of an explicit time integration scheme. The eigenmodes satisfy

$$K\dot{u}_{iI} = B_{jI}\bar{T}^{\nabla}_{ij} \tag{30}$$

where K is the modal stiffness, or eigenvalue, and $\dot{u}_{iI}$ is the modal shape, or eigenvector. For a lumped mass in which the element mass is distributed equally among the 8 nodes, the modal frequency is related to the modal stiffness by

$$K = \frac{\rho V}{8}\omega^2 \tag{31}$$

where ρ is the density. Equations (5), (12) and (29), when substituted into the right hand side of (30), yield the standard eigenvalue problem from which K is obtained.

Solutions satisfying condition (30) are detailed in Reference 13, where it is shown that the maximum stiffness and frequency are bounded by:

$$(\lambda + 2\mu)\frac{B_{iI}B_{iI}}{V} \geqslant K_{\max} \geqslant \frac{\lambda + 2\mu}{3}\frac{B_{iI}B_{iI}}{V} \tag{32}$$

$$8\frac{\lambda + 2\mu}{\rho}\frac{B_{iI}B_{iI}}{V^2} \geqslant \omega^2_{\max} \geqslant \frac{8}{3}\frac{\lambda + 2\mu}{\rho}\frac{B_{iI}B_{iI}}{V^2} \tag{33}$$

It is well known that a central difference time integration scheme is stable if

$$\Delta t \leqslant \frac{2}{\omega_{\max}}[\sqrt{(1-\varepsilon^2)} - \varepsilon] \tag{34}$$

where ε is the fraction of critical damping in the highest frequency. Stability of the explicit scheme is thus assured if

$$\Delta t \leqslant V\sqrt{\left[\frac{\rho}{2(\lambda + 2\mu)B_{iI}B_{iI}}\right]}[\sqrt{(1-\varepsilon^2)} - \varepsilon] \tag{35}$$

ANTI-HOURGLASSING

The mean stress–strain formulation considers only a fully linear velocity field. The remaining portion of the nodal velocity field is the so-called hourglass field. Excitation of these modes may lead to severe, unresisted mesh distortion. We now present a method for isolating the hourglass modes so that they may be treated independently of the rigid body and uniform strain modes.

A fully linear velocity field for the hexahedron can be described by

$$\dot{u}_i^{\mathrm{LIN}} = \bar{\dot{u}}_i + \bar{\dot{u}}_{i,j}(x_j - \bar{x}_j) \tag{36}$$

The mean co-ordinates $\bar{x}_i$ correspond to the centre of the nodes and are defined as

$$\bar{x}_i = \tfrac{1}{8}x_{iI}\Sigma_I \tag{37}$$

The mean translational velocity is similarly defined by

$$\bar{\dot{u}}_i = \tfrac{1}{8}\dot{u}_{iI}\Sigma_I \tag{38}$$

The linear portion of the nodal velocity field may be expressed by specializing equation (36) to the nodes as follows:

$$\dot{u}_{iI}^{\mathrm{LIN}} = \bar{\dot{u}}_i\Sigma_I + \bar{\dot{u}}_{i,j}(x_{jI} - \bar{x}_j\Sigma_I) \tag{39}$$

where Σ_I is used to maintain consistent index notation and indicates that $\mathring{\dot{u}}_i$ and $\bar{x}_i$ are independent of position within the element. We may prove, using equations (39), (38), (26), (12) and (15), the following indentities:

$$\dot{u}_{iI}\Sigma_I = \dot{u}_{iI}^{\mathrm{LIN}}\Sigma_I = 8\mathring{\dot{u}}_i \tag{40}$$

$$\dot{u}_{iI}B_{jI} = \dot{u}_{iI}^{\mathrm{LIN}}B_{jI} = V\mathring{\dot{u}}_{i,j} \tag{41}$$

One would expect the above conditions to hold since the same mean velocity and velocity gradient should be obtained whether or not we consider the linear strain rates (nonlinear velocities).

The hourglass field $\dot{u}_{iI}^{\mathrm{HG}}$ may now be defined by removing the linear portion of the nodal velocity field:

$$\dot{u}_{iI}^{\mathrm{HG}} = \dot{u}_{iI} - \dot{u}_{iI}^{\mathrm{LIN}} \tag{42}$$

Equations (42), (40) and (41) prove that Σ_I and B_{iI} are orthogonal to the hourglass field:

$$\dot{u}_{iI}^{\mathrm{HG}}\Sigma_I = 0 \tag{43}$$

$$\dot{u}_{iI}^{\mathrm{HG}}B_{jI} = 0 \tag{44}$$

Furthermore, since equations (26) and (27) imply that the B-matrix is a linear combination of the volumetric base vectors, Λ_{iI}, the last condition may be stated equivalently as

$$\dot{u}_{iI}^{\mathrm{HG}}\Lambda_{jI} = 0 \tag{45}$$

Equations (43) and (45) show that the hourglass field is orthogonal to all the base vectors in Table I except the hourglass base vectors. Therefore, $\dot{u}_{iI}^{\mathrm{HG}}$ may be expanded as a linear combination of the hourglass base vectors as follows:

$$\dot{u}_{iI}^{\mathrm{HG}} = \frac{1}{\sqrt{8}}\dot{q}_{i\alpha}\Gamma_{\alpha I} \tag{46}$$

The hourglass modal velocities are represented by $\dot{q}_{i\alpha}$ above (the leading constant is added to normalize $\Gamma_{\alpha I}$). We now define the hourglass shape vector $\gamma_{\alpha I}$ such that

$$\dot{q}_{i\alpha} = \frac{1}{\sqrt{8}}\dot{u}_{iI}\gamma_{\alpha I} \tag{47}$$

By substituting (39), (42), and (47) into (46), then multiplying by $\Gamma_{\alpha I}$ and using the orthogonality of the base vectors, we obtain the following:

$$\dot{u}_{iI}\Gamma_{\alpha I} - \mathring{\dot{u}}_{i,j}x_{jI}\Gamma_{\alpha I} = \dot{u}_{iI}\gamma_{\alpha I} \tag{48}$$

With the definition of $\mathring{\dot{u}}_{i,j}$ (12) we can eliminate the nodal velocities above. As a result, we can compute $\gamma_{\alpha I}$ from the following expression:

$$\gamma_{\alpha I} = \Gamma_{\alpha I} - \frac{1}{V}B_{iI}x_{iJ}\Gamma_{\alpha J} \tag{49}$$

The difference between the hourglass base vectors $\Gamma_{\alpha I}$ and the hourglass shape vectors $\gamma_{\alpha I}$ is very important. They are identical if and only if the hexahedron is a parallelepiped. For a general shape, $\Gamma_{\alpha I}$ is orthogonal to B_{jI} while $\gamma_{\alpha I}$ is orthogonal to the linear velocity field $\dot{u}_{iI}^{\mathrm{LIN}}$. While $\Gamma_{\alpha I}$ defines the hourglass pattern, $\gamma_{\alpha I}$ is necessary to accurately detect hourglassing.

We explored two methods for alleviating hourglass difficulties. The first approach is to apply artificial damping to the hourglass modes. The intent of this method is to allow some hourglassing, but prevent violent oscillations. A shortcoming of the hourglass damping approach is that, since there is no stiffness in the hourglass modes, mesh distortion in these modes is permanent.

A more successful approach to combat hourglassing is to use an artificial stiffness which allows only mild hourglassing. Unlike damping, hourglass stiffness does not attenuate global modes. Of course, artificial stiffness and damping could be combined, but we found no evidence that additional damping provides any improvement.

For the purpose of controlling the hourglass modes, we define generalized forces $Q_{i\alpha}$ which are conjugate to $\dot{q}_{i\alpha}$, so that the rate of work is given by

$$\dot{u}_{iI} f_{iI}^{\mathrm{HG}} = Q_{i\alpha} \dot{q}_{i\alpha} \tag{50}$$

for arbitrary $\dot{u}_{iI}$. Using equation (47), it follows that the contribution of the hourglass resistance to the nodal forces is given by

$$f_{iI}^{\mathrm{HG}} = \frac{1}{\sqrt{8}} Q_{i\alpha} \gamma_{\alpha I} \tag{51}$$

Two types of hourglass resistance will be used here: artificial damping and artificial stiffness. The damping and stiffness are defined in terms of the maximum frequency and stiffness of the element, so that

$$Q_i = 2\varepsilon\omega_{\max}\left(\frac{\rho V}{8}\right)\dot{q}_{i\alpha} + \kappa K_{\max} q_{i\alpha} \tag{52}$$

where ε and κ are the damping and stiffness parameters, respectively. Lower bounds given by equations (32) and (33) are used for the maximum frequency and stiffness, so that the equations for the hourglass resistances are

$$Q_{i\alpha} = \varepsilon \sqrt{\left[\frac{\rho(\alpha + 2\mu) B_{iI} B_{iI}}{6}\right]} \dot{q}_{i\alpha} \tag{53}$$

$$\dot{Q}_{i\alpha} = \kappa \frac{\lambda + 2\mu}{3} \frac{B_{iI} B_{iI}}{V} \dot{q}_{iI} \tag{54}$$

for the artificial damping and artificial stiffness, respectively. The rate form is used for the stiffness instead of the total form given in equation (52) because it is more suitable for large deformation problems. The damping coefficient ε is defined so that equation (35) always gives a conservative estimate of the stable time step.

Observe that the nodal anti-hourglass forces (51) have the shape of $\gamma_{\alpha I}$, rather than $\Gamma_{\alpha I}$. This fact is essential since the anti-hourglass forces should be orthogonal to the linear velocity field, so that no energy is transferred to or from the rigid body and uniform strain modes by the anti-hourglass scheme.

QUADRILATERAL ELEMENT

Previously in this paper we have focused solely on the 3-D hexahedron. Expressions relevant to the 2-D quadrilateral could be generated by degrading the hexahedron. However, deriving expressions for the quadrilateral is far less complicated, which allows important aspects to be more clearly illustrated. Towards this end, we now present an independent derivation for the quadrilateral element.

The 2-D isoparametric shape functions map the unit square in $\xi-\eta$ to an arbitrary quadrilateral in x–y, as shown in Figure 2. The shape functions ϕ_I are given, analogous to

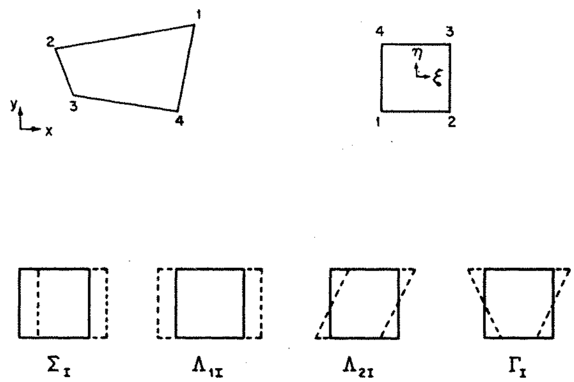

Figure 2. Quadrilateral and its displacement modes; hourglass modes are Γ_I

equation (7), below. Note that throughout this section, lowercase and uppercase subscripts have ranges of two and four, respectively. Table II defines the quadrilateral base vectors, as Table I does for the hexahedron.

$$\phi_I = \tfrac{1}{4}\Sigma_I + \tfrac{1}{2}\xi\Lambda_{1I} + \tfrac{1}{2}\eta\Lambda_{2I} + \xi\eta\Gamma_I \tag{55}$$

Table II

Node	ξ	η	Σ_I	Λ_{1I}	Λ_{2I}	Γ_I
1	$-\frac{1}{2}$	$-\frac{1}{2}$	1	−1	−1	1
2	$\frac{1}{2}$	$-\frac{1}{2}$	1	1	−1	−1
3	$\frac{1}{2}$	$\frac{1}{2}$	1	1	1	1
4	$-\frac{1}{2}$	$\frac{1}{2}$	1	−1	1	−1

We define the B-matrix with respect to element area A, since thickness is assumed constant, as below:

$$B_{iI} = \int_A \phi_{I,i}\,\mathrm{d}A \tag{56}$$

Analogous to equations (15) and (16), the B-matrix is related to element area by

$$x_{iI}B_{jI} = A\delta_{ij} \tag{57}$$

$$B_{iI} = \frac{\partial A}{\partial x_{iI}} \tag{58}$$

The mean velocity gradient and nodal forces are computed as below:

$$\dot{u}_{i,j}=\frac{1}{A}\dot{u}_{iI}B_{jI} \tag{59}$$

$$f_{iI}=t\bar{T}_{ij}B_{jI} \tag{60}$$

where t is the element thickness.

Analogous to equation (17), the element area is defined in terms of the Jacobian J:

$$A=\int_{-1/2}^{1/2}\int_{-1/2}^{1/2}J\,\mathrm{d}\eta\,\mathrm{d}\xi \tag{61}$$

where

$$J=\frac{\partial x}{\partial \xi}\frac{\partial y}{\partial \eta}-\frac{\partial x}{\partial \eta}\frac{\partial y}{\partial \xi} \tag{62}$$

Therefore, equation (61) may be written as

$$A=x_Iy_JC_{IJ} \tag{63}$$

where

$$C_{IJ}=\int_{-1/2}^{1/2}\int_{-1/2}^{1/2}\left(\frac{\partial \phi_I}{\partial \xi}\frac{\partial \phi_J}{\partial \eta}-\frac{\partial \phi_I}{\partial \eta}\frac{\partial \phi_J}{\partial \xi}\right)\mathrm{d}\eta\,\mathrm{d}\xi \tag{64}$$

In light of equation (55), the above integration involves at most bilinear functions. Therefore, only the constant term does not vanish. Similar to the form of equation (23), we obtain

$$C_{IJ}=\tfrac{1}{4}(\Lambda_{1I}\Lambda_{2J}-\Lambda_{2I}\Lambda_{1J}) \tag{65}$$

Note that C_{IJ} is antisymmetric:

$$C_{IJ}=-C_{JI} \tag{66}$$

Evaluating equation (65) we obtain the following explicit representation for C_{IJ}:

$$C_{IJ}=\frac{1}{2}\begin{bmatrix}0 & 1 & 0 & -1\\ -1 & 0 & 1 & 0\\ 0 & -1 & 0 & 1\\ 1 & 0 & -1 & 0\end{bmatrix} \tag{67}$$

Substituting the above result into (63), we get the familiar expression for the area of a quadrilateral:

$$A=\tfrac{1}{2}[(x_3-x_1)(y_4-y_2)+(x_2-x_4)(y_3-y_1)] \tag{68}$$

By applying equation (58), the B-matrix may be expressed as

$$B_{iI}=C_{IJ}\begin{bmatrix}y_J\\ -x_J\end{bmatrix}=\frac{1}{2}\begin{bmatrix}(y_2-y_4) & (y_3-y_1) & (y_4-y_2) & (y_1-y_3)\\ (x_4-x_2) & (x_1-x_3) & (x_2-x_4) & (x_3-x_1)\end{bmatrix} \tag{69}$$

The mean stress approach gives identical results as one-point quadrature for the quadrilateral since the Jacobian (62) is at most bilinear.

The hourglass modes for the quadrilateral may be treated by procedures analogous to the methods derived for the hexahedron. The hourglass velocities are defined as

$$\dot{q}_i=\tfrac{1}{2}\dot{u}_{iI}\gamma_I \tag{70}$$

The hourglass shape vector is computed as per equation (49):

$$\gamma_I = \Gamma_I - \frac{1}{A} B_{iI} x_{iJ} \Gamma_J \tag{71}$$

The above expression is simple enough to be written explicitly as below:

$$\gamma_I = \frac{1}{4A}\begin{bmatrix} x_2(y_3-y_4)+x_3(y_4-y_2)+x_4(y_2-y_3) \\ x_3(y_1-y_4)+x_4(y_3-y_1)+x_1(y_4-y_3) \\ x_4(y_1-y_2)+x_1(y_2-y_4)+x_2(y_4-y_1) \\ x_1(y_3-y_2)+x_2(y_1-y_3)+x_3(y_2-y_1) \end{bmatrix} \tag{72}$$

The anti-hourglass forces are computed by

$$f_{iI}^{\mathrm{HG}} = \tfrac{1}{2} Q_i \gamma_I \tag{73}$$

The maximum stiffness and frequency, in contrast to equations (32) and (33), are bounded by[13]

$$(\lambda + 2\mu)\frac{tB_{iI}B_{iI}}{A} \geq K_{\max} \geq \frac{\lambda + 2\mu}{2}\frac{tB_{iI}B_{iI}}{A} \tag{74}$$

$$4\frac{\lambda + 2\mu}{\rho}\frac{B_{iI}B_{iI}}{A^2} \geq \omega_{\max}^2 \geq 2\frac{\lambda + 2\mu}{\rho}\frac{B_{iI}B_{iI}}{A^2} \tag{75}$$

Therefore, artificial hourglass damping resistances or stiffness resistance rates are defined by the following two expressions, respectively:

$$Q_i = \varepsilon t\sqrt{\left(\frac{\rho(\lambda + 2\mu)B_{iI}B_{iI}}{2}\right)}\,\dot{q}_i \tag{76}$$

$$\dot{Q}_i = \kappa t\frac{\lambda + 2\mu}{2}\frac{B_{iI}B_{iI}}{A}\dot{q}_i \tag{77}$$

Finally, the explicit stability limit (35) becomes

$$\Delta t \leq A\sqrt{\frac{\rho}{(\lambda + 2\mu)B_{iI}B_{iI}}} \tag{78}$$

NUMERICAL EXAMPLES

The best illustration of hourglass effects arises when modelling the first mode of a beam. This is a severe problem for hourglassing as no deflection is possible without exciting hourglass modes.

The first test problem shown in Figure 3, is a beam which is simply supported at both ends; midspan symmetry was used as shown. A uniform step load, which yielded maximum deflections on the order of the depth of the beam, was applied. A large deflection problem was considered to show that our anti-hourglass techniques are effective in a nonlinear situation. Figures 3–9 depict the solution with no anti-hourglass control, and various magnitudes of anti-hourglass viscosity ε and elastic hourglass control κ.

The first sequence, Figure 3, shows the gross mesh distortion caused by the unstable global mode. Obviously, the solution rapidly becomes meaningless. Observe also that an unresisted global mode persists even though the element hourglass mode shapes change drastically. In

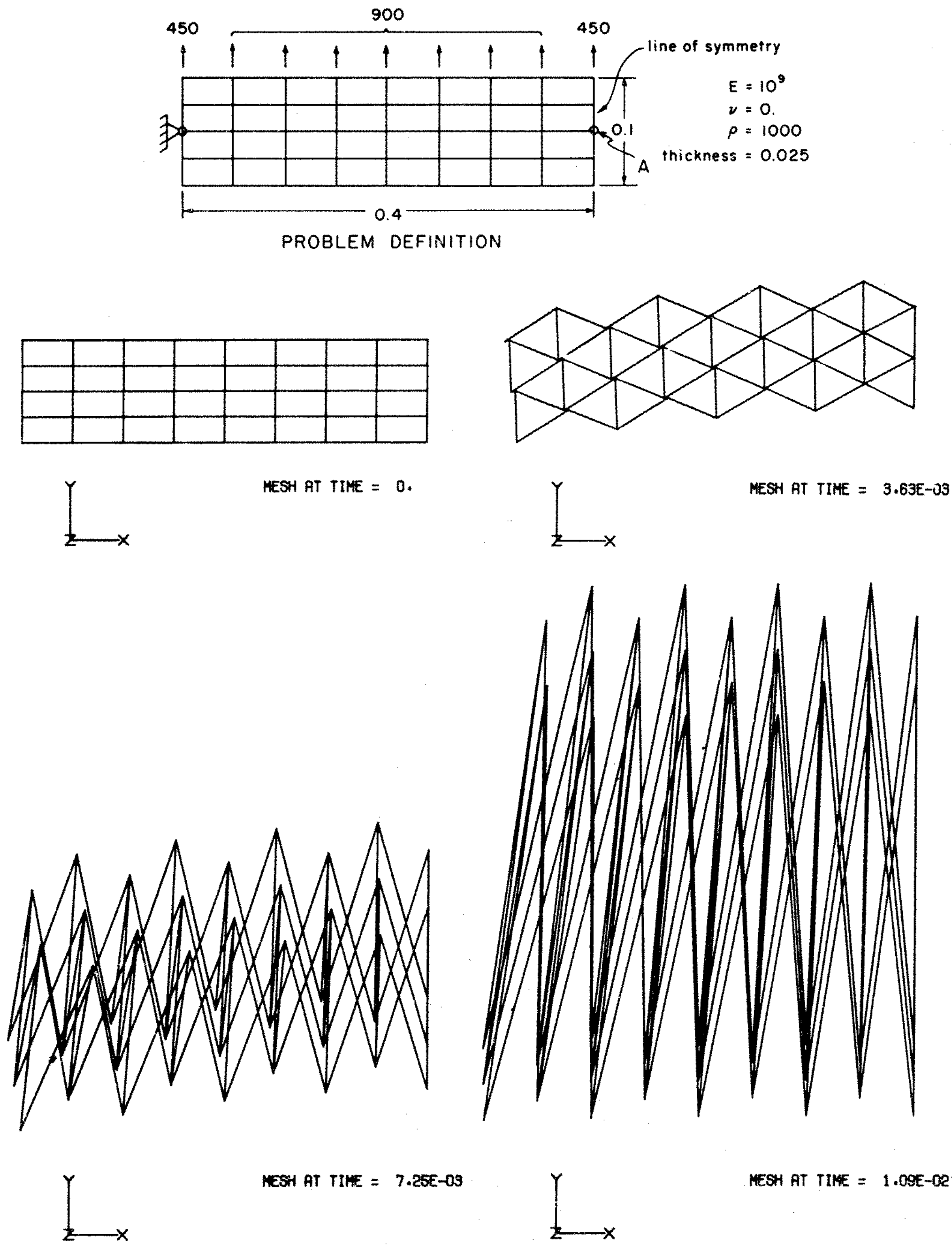

Figure 3. Uniformly loaded, simply supported beam; problem definition and mesh deformation with no anti-hourglassing

other words, the mesh does not stabilize as it distorts. Figure 4 shows the displacement of the midpoint; comparison with the solutions of Figure 7 shows significant error in this unstable solution.

Figure 5 demonstrates that anti-hourglass viscosity simply slows down the hourglass distortion, and does not stabilize the solution. The step load excitation, in the absence of any restoring force, induces the global hourglass mode to deform without bound. By increasing the damping ratio we were able to obtain a reasonable solution, at least through one period. However, a significant penalty was paid since for the parameters used in Figure 6, the stable time step is about 60 per cent of the time step for the undamped mesh. Interestingly, the period and attenuation in Figure 7 do not differ greatly, while the damping ratio differs by a factor of five. Both trends indicate that the global hourglass pattern may be damped almost independently of

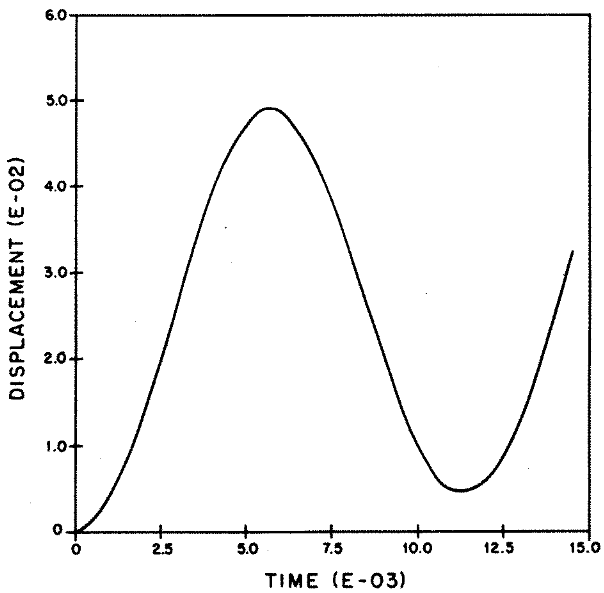

Figure 4. Displacement of point A (see Figure 3) with no anti-hourglassing

the beam mode. This result is a consequence of the element hourglass modes orthogonality to the rigid body and uniform stress modes.

Figure 8 demonstrates that even a small anti-hourglass stiffness stabilizes the solution. Figure 9 shows the solution with $\kappa = 0{\cdot}125$. This value of κ was chosen so that the hourglass modes in the x-direction (those which appear in the beam solution) are integrated as accurately as possible, in the manner of Kosloff and Frazier.[10] Figure 9 also shows that over-stiffening the hourglass modes by a factor of four causes a 7 per cent reduction in the period. This result indicates that, in contrast to damping, too much anti-hourglass stiffness can adversely affect the solution. However, for low stiffness ratios, the effect on the solution is insignificant. Furthermore, it should be noted that elastic hourglass control cannot decrease the explicit stability limit for ratios not exceeding unity.

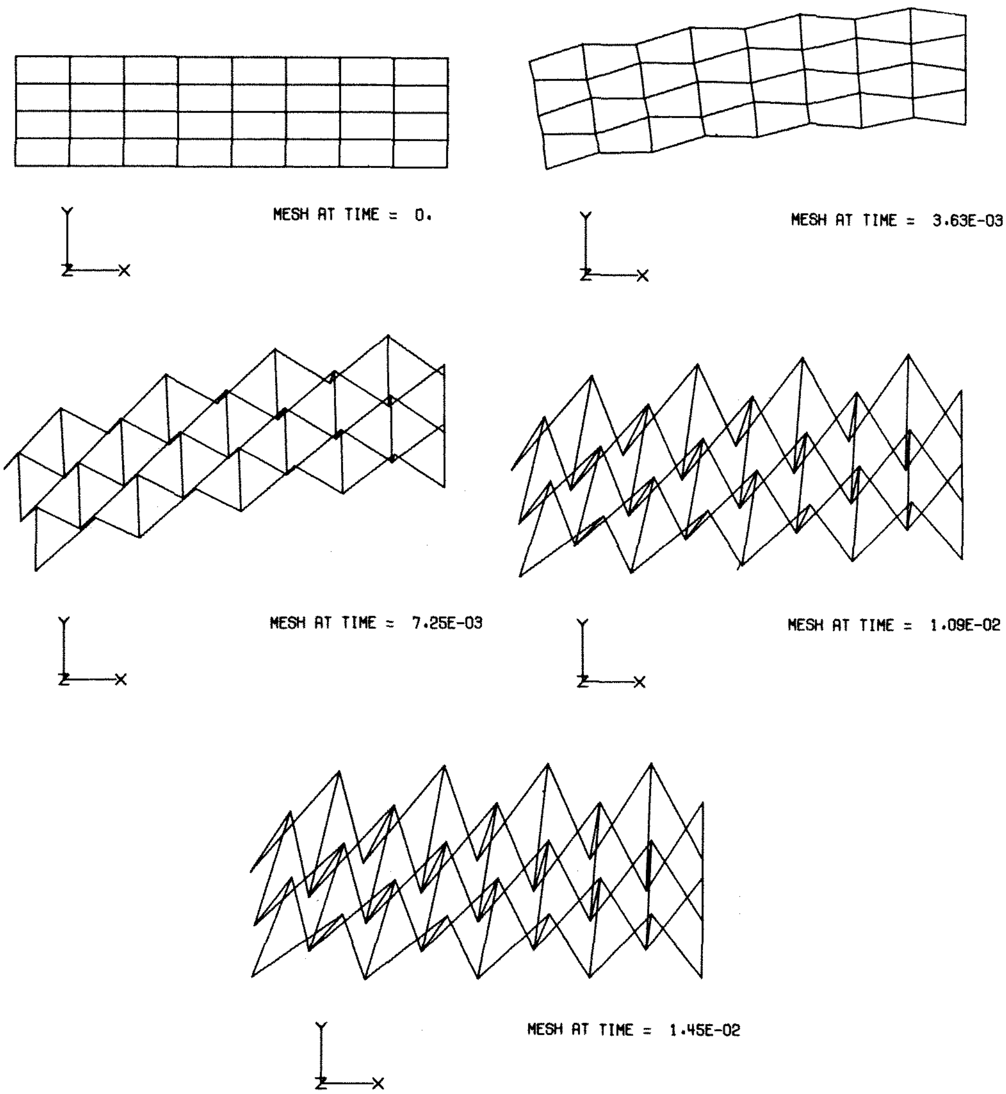

Figure 5. Mesh deformation with anti-hourglass damping $\varepsilon = 0{\cdot}01$

Global hourglass patterns are heavily dependent upon boundary constraints. In fact, constraints often preclude the existence of unstable global modes. The next test problem illustrates this effect. In this test problem, the support conditions of the beam were changed to a 'built-in' cantilever, as shown in Figure 10. The beam was again subjected to a uniform load, but the load was reduced so that the response was linear. Figure 10 shows that no instabilities occurred. (Note that the displacements were greatly exaggerated for the mesh plots.) Figure 11 shows the solution with no anti-hourglassing and the 'optimum' (as in the previous problem) anti-hourglass stiffness ratio, respectively. The first case gave a period 8·5 per cent in excess of the beam equation solution, while the corresponding error for the second case was 5·2 per cent.

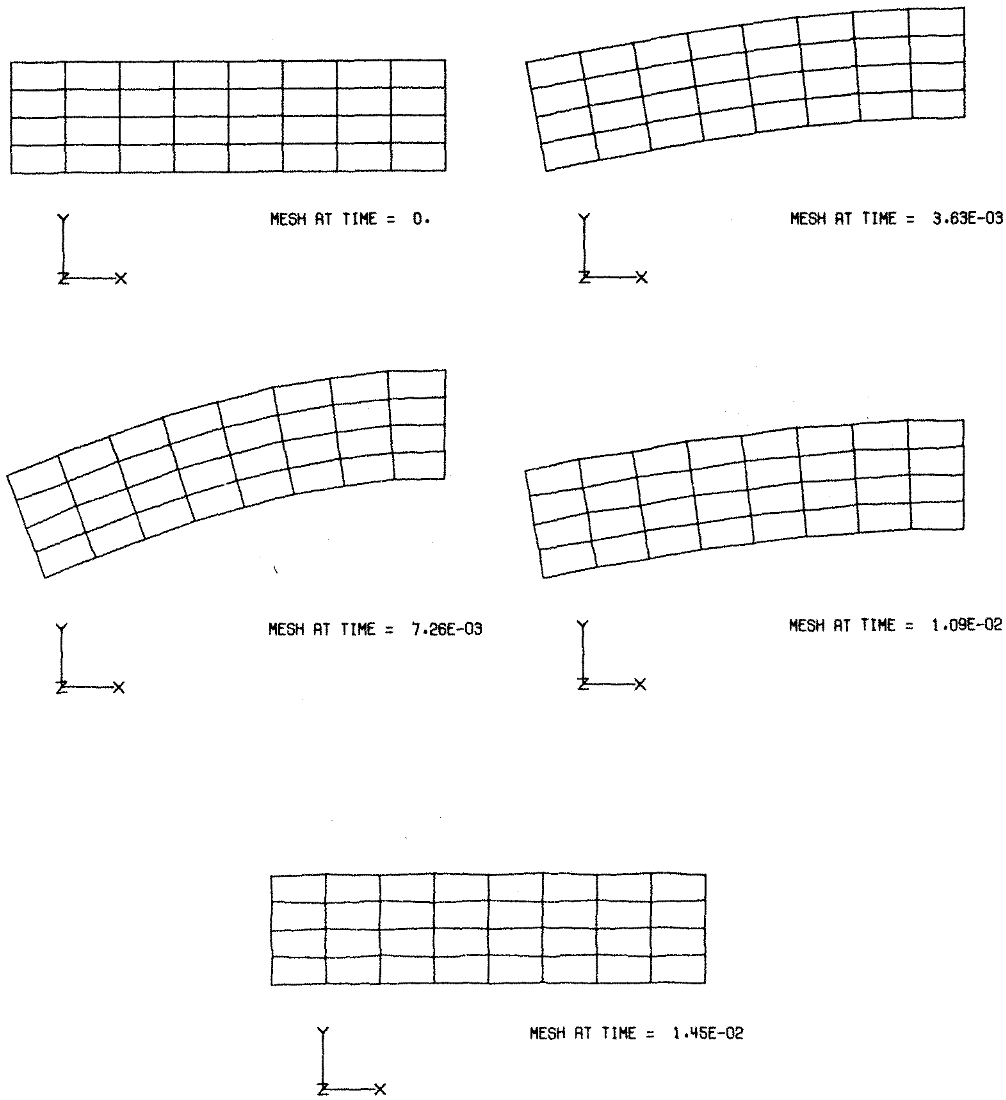

Figure 6. Mesh deformation with anti-hourglass damping $\varepsilon = 0{\cdot}5$

The last sample problem models a spherical pressure wave in an ideal fluid. The mesh is shown in Figure 12. The spherical cavity inside the mesh was loaded by a step pressure, which causes an out-going wave. An incoming wave subsequently develops upon reflection from the outside boundary of the mesh. This test problem was designed to check the performance of the one-point hexahedron. Only one octant was discretized since symmetry was assumed. Twelve elements were used across the spherical surface and fifteen in the radial direction.

In Figure 12, the pressure midway through the fluid is compared with the analytic solution. Disregarding the aliasing effect, which is a result of dispersion and of the finite cut-off frequency of the mesh, the numerical solution agrees well with the analytic.

The hourglass modes were not excited in the spherical wave problem. Consequently, elastic hourglass control had no appreciable influence on the solution. Anti-hourglass viscosity did not alter the solution of the spherical wave problem nor the cantilever beam problem, except to lower the stable time step. These results are consequences of the orthogonality of the hourglass and linear deformation modes. If this conditon were not satisfied, it would be possible to inadvertently excite the hourglass modes by hourglass control in a situation where they may not otherwise be troublesome.

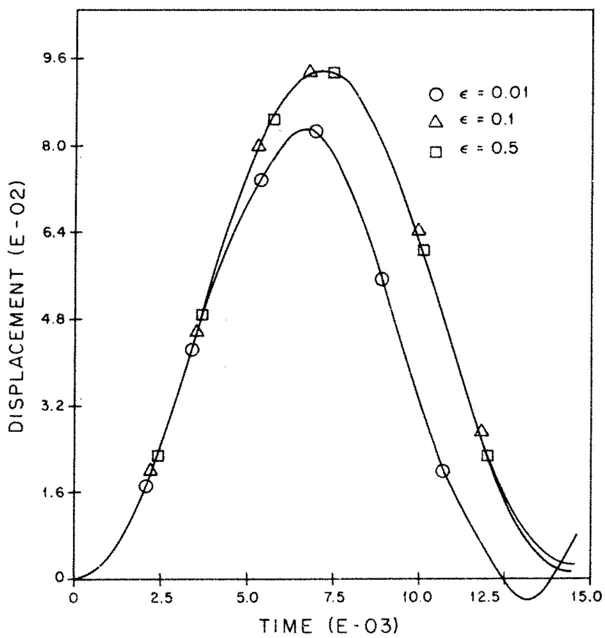

Figure 7. Displacement of point A (see Figure 3) for various values of anti-hourglass damping ε

DISCUSSION

The linear strain modes of isoparametric elements offer little additional accuracy in most transient analysis problems. We, therefore, consider integrating these modes not to be cost-effective in such applications, especially in nonlinear cases. The one-point integration scheme with hourglass control presented here achieves greater speed while still assuring stability and convergence.

Using Gauss quadrature to stabilize the element hourglass modes increases computational burden roughly by a factor of four with the quadrilateral and by a factor of eight with the hexahedron. In contrast, the anti-hourglass procedure presented here can precisely isolate and stabilize the hourglass modes while increasing computations by only 30–40 per cent.

Generally, boundary conditions eliminate global hourglass modes. The added burden of hourglass control should be avoided if it is known *a priori* that instabilities will not arise. However, it is safe to apply the anti-hourglass procedures when stability is in doubt, without risk

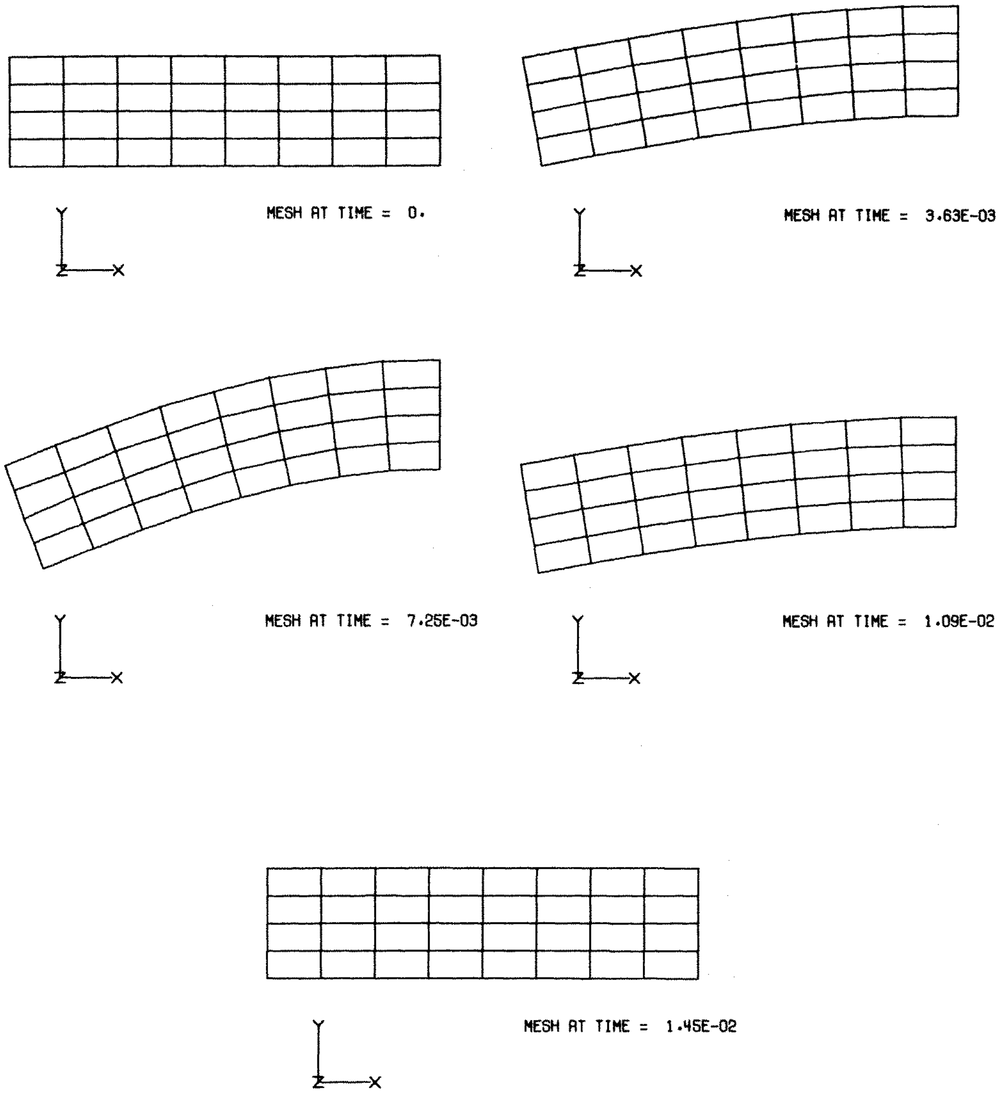

Figure 8. Mesh deformation with anti-hourglass stiffness $\kappa = 0{\cdot}01$

of diminishing the accuracy of the solution, due to the enforced independence of the hourglass modes.

The hourglass 'twist' modes of the hexahedron should never present a problem. However, it is impossible to separate these modes from the 'bending' hourglass modes for a general hexahedron. It is, in any case, prudent to treat all hourglass modes identically.

Viscous hourglass control has two advantages over elastic control in practical applications:

1. Low frequency response modes are affected little by even heavy damping.
2. No additional variables need be stored.

The disadvantages of viscous hourglass control which are avoided by elastic control are:

1. Stability is not guaranteed by damping a stressless global mode.
2. Mesh distortion is permanent in the absence of restoring forces.
3. The explicit time step stability limit is lowered substantially by damping.

In consideration of the above points, we judge elastic hourglass control preferable to viscous control.

One danger in applying elastic hourglass control is that if the stiffness ratio is too large, 'locking' of the elements may result. Small stiffness ratios, on the other hand, ensure stability while not adversely affecting the solution. It should be stressed that anti-hourglass stiffness is strictly for control of mesh stability; therefore, small stiffness ratios are recommended.

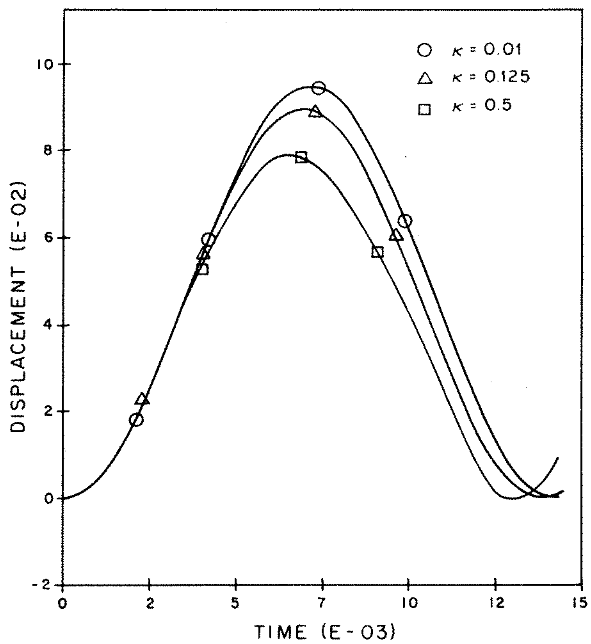

Figure 9. Displacement of point A (see Figure 3) for various values of anti-hourglass stiffness κ

CONCLUSION

A one-point integration method and an associated hourglass control scheme were developed. The important aspects of these techniques are:

1. Hourglass shapes are orthogonal to the uniform strain and rigid body modes.
2. The shape vectors are computed directly, i.e. no solution of equations is necessary.
3. The volume and uniform strain states of a hexahedron are integrated accurately without an averaging scheme.

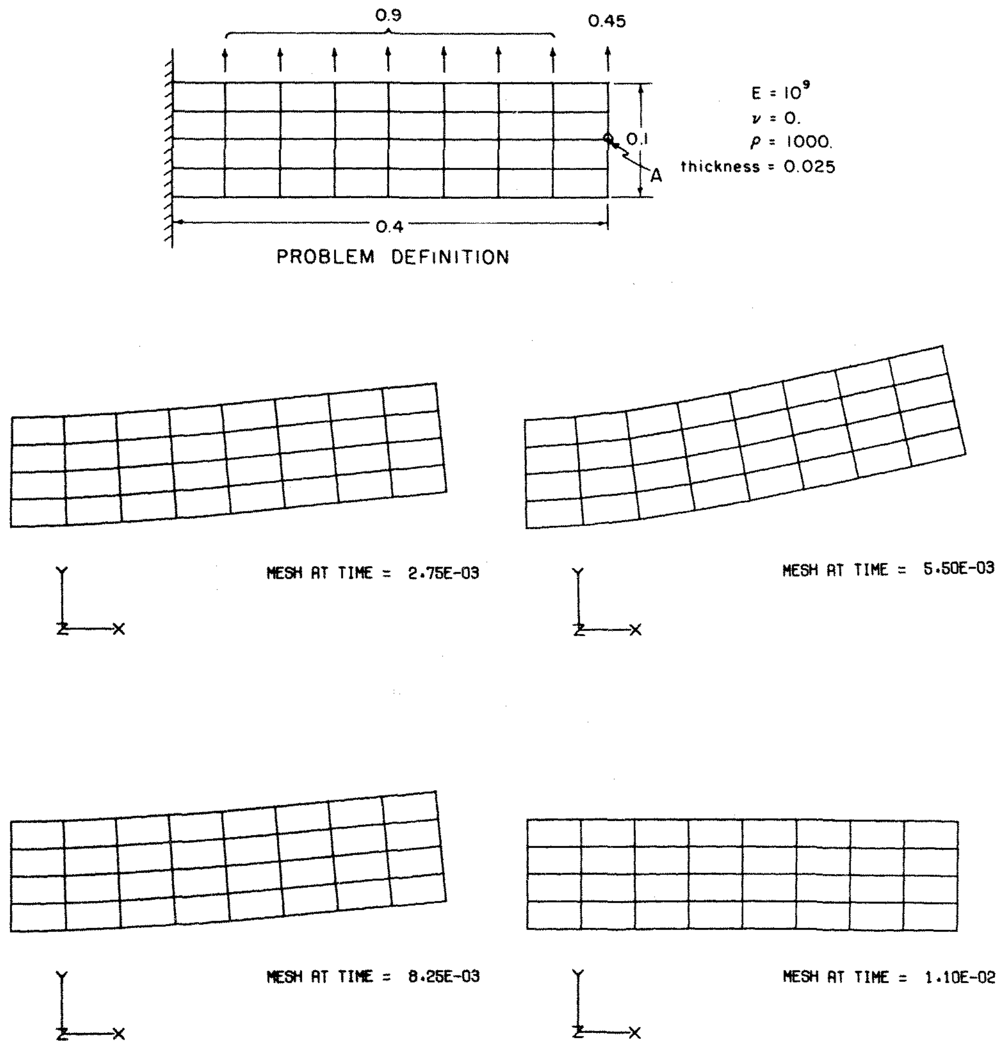

Figure 10. Uniformly loaded cantilever beam; problem definition and mesh deformation with no anti-hourglassing

Two forms of hourglass control were tested and evaluated:

1. Viscous control (anti-hourglass viscosity).
2. Elastic control (anti-hourglass stiffness).

Of these two methods, the latter was found to be superior in achieving mesh stability. The first mode of a beam was presented as a good check problem for the hourglass control schemes and illustrates their comparative behaviour.

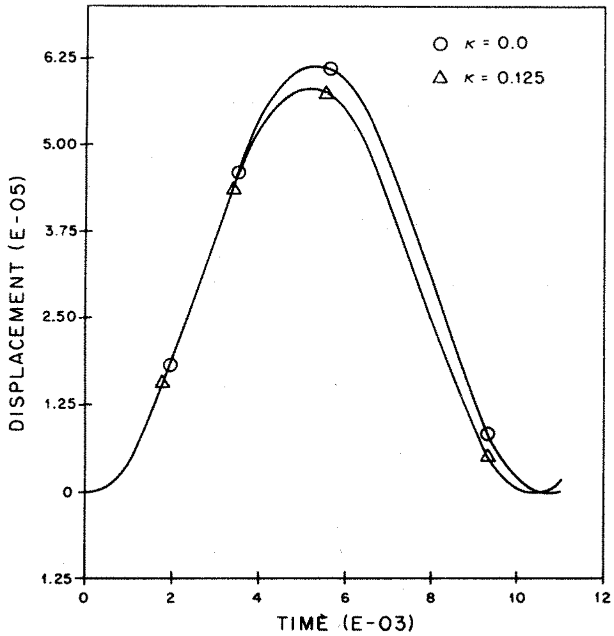

Figure 11. Displacement of point A (see Figure 10) for anti-hourglass stiffness $\kappa = 0$ and 0·125

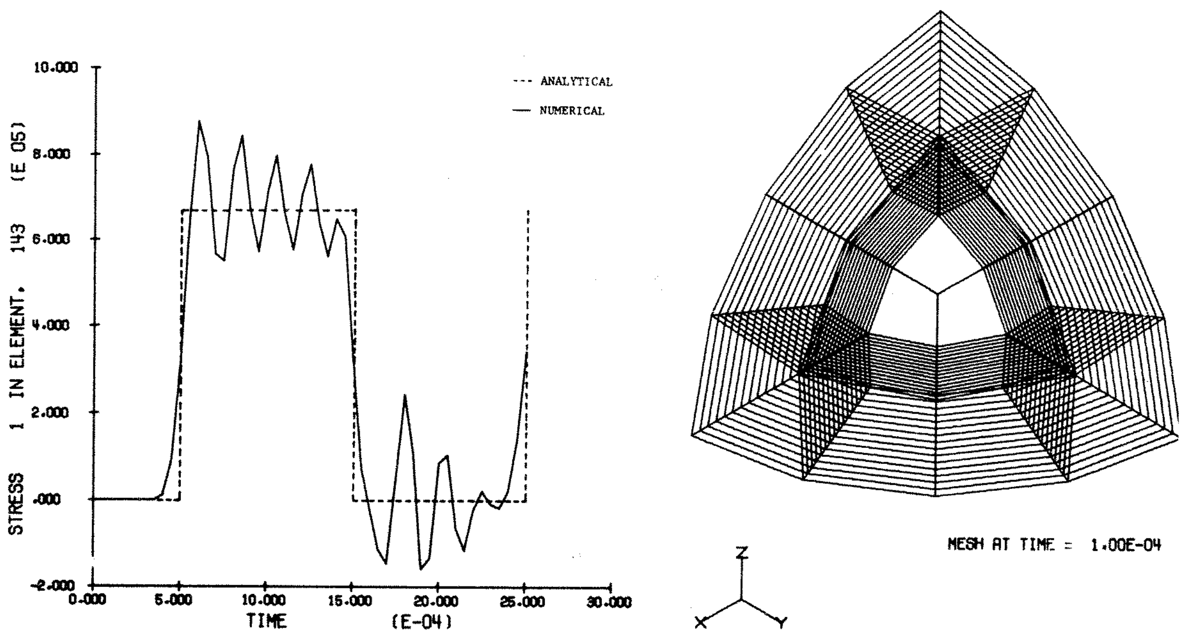

Figure 12. Spherical wave problem; undeformed mesh and midpoint pressure

APPENDIX I

Computation of the B-matrix (22) and element volume (19) for the hexahedron requires evaluation of the coefficient array C_{IJK} as per equation (23). Since C_{IJK} has the alternator properties given in equation (21), only 56 (the combination of eight nodes taken three at a time) distinct non-zero terms are possible. However, the volume must be independent of the selection of node 1, which implies that C_{IJK} is invariant if the nodes are permuted according to Table III. Consequently, only 21 (the combination of seven nodes taken two at a time) terms may be independent. Furthermore, once node 1 is selected, three orientations of the node numbering system are possible, as given by the permutation Table IV. Therefore, only seven terms of C_{IJK} need be evaluated.

Table III. Nodal permutations

1	2	3	4	5	6	7	8
2	3	4	1	6	7	8	5
3	4	1	2	7	8	5	6
4	1	2	3	8	5	6	7
5	8	7	6	1	4	3	2
6	5	8	7	2	1	4	3
7	6	5	8	3	2	1	4
8	7	6	5	4	3	2	1

Table IV. Nodal permutations

1	2	3	4	5	6	7	8
1	4	8	5	2	3	7	6
1	5	6	2	4	8	7	3

Table V

I	J	K	C_{IJK}
1	2	3	−1/12
1	2	5	+1/12
1	2	6	+1/12
1	2	7	0
1	2	8	0
1	3	5	0
1	3	6	0

Table VI. Co-ordinate axes permutations

1	2	3
2	3	1
3	1	2

Seven independent terms of C_{IJK} are listed in Table III. These terms may be evaluated via equation (23) and Table I. Only three of these seven terms do not vanish, as indicated in Table V. All other non-zero terms of C_{IJK} are found by permuting the nodes according to Table III and using the alternator properties (21). Alternatively, the non-zero terms may be generated by applying asymmetry, $C_{IKJ} = -C_{IJK}$, to Table V, then permuting according to Tables IV and III, successively. The latter scheme straightforwardly results in formulae for computing the B-matrix (22).

The first term of B_{iI} is expressed below in nested form. Other terms of B_{iI} are evaluated using the same formula after permuting the nodes according to Table III and, subsequently, permuting the co-ordinate axes according to Table VI. The element volume is most easily computed by contracting the B-matrix and nodal co-ordinates as per equation (15):

$$\begin{aligned} B_{11} = \tfrac{1}{12}[&y_2((z_6-z_3)-(z_4-z_5))+y_3(z_2-z_4) \\ &+y_4((z_3-z_8)-(z_5-z_2))+y_5((z_8-z_6)-(z_2-z_4)) \\ &+y_6(z_5-z_2)+y_8(z_4-z_5)] \end{aligned} \tag{79}$$

APPENDIX II

```
      SUBROUTINE FHEX(NDF,XX,V,F,NODE,P,E)
      DIMENSION XX(NDF,1),V(NDF,1),F(NDF,1),NODE(8)
      COMMON /LOCAL/ X(8,3),B(8,3),VOL,AHR
      COMMON /TIME/ T,DT,NSTEP,MSTEP
C
C     INTERNAL FORCE ROUTINE FOR HEXAHEDRON (IDEAL FLUID)
C     D. P. FLANAGAN        7/18/80
C
C     DESCRIPTION:
C          THE INTERNAL FORCES FOR A HEXAHEDRON ARE CALCULATED FROM THE
C     ELEMENT MEAN PRESSURE AND B-MATRIX.  THE B-MATRIX IS DEFINED IN
C     SUBROUTINE BOHEX.  THE PRESSURE RATE IS COMPUTED FROM THE VOLUME
C     RATE AND BULK MODULUS.
C          THIS ROUTINE COUPLES WITH IHEX.
C
C     VARIABLES:
C     NAME      TYPE       DESCRIPTION
C
C     NDF       INTEGER    NUMBER OF DEGREES OF FREEDOM (3)
C     XX        REAL       GLOBAL COORDINATES
C     V         REAL       GLOBAL VELOCITIES
C     F         REAL       GLOBAL FORCES
C     NODE      INTEGER    ELEMENT NODE NUMBERS
C     P         REAL       ELEMENT PRESSURE
C     E         REAL       BULK MODULUS
C     X         REAL       ELEMENT COORDINATES
C     B         REAL       B-MATRIX
C     VOL       REAL       ELEMENT VOLUME
C     DT        REAL       TIME INCREMENT
C     R         REAL       VOLUME RATE (* VOLUME)
C
C
C     EXTRACT ELEMENT COORDINATES
C
      DO 10 J=1,8
      N=NODE(J)
      DO 10 I=1,3
 10   X(J,I)=XX(I,N)
C
C     FIND B-MATRIX
C
      CALL BOHEX(B(1,1),X(1,2),X(1,3))
      CALL BOHEX(B(1,2),X(1,3),X(1,1))
      CALL BOHEX(B(1,3),X(1,1),X(1,2))
C
C     CALCULATE VOLUME AND VOLUME RATE
C
```

```
      R=VOL=0.
      DO 30 I=1,8
      N=NODE(I)
      DO 20 J=1,3
 20   R=R+B(I,J)*V(J,N)
 30   VOL=VOL+B(I)*X(I)
C
C     UPDATE PRESSURE
C
      P=P-DT*E*R/VOL
C
C     ADD ELEMENT FORCES TO GLOBAL ARRAY
C
      DO 40 J=1,8
      N=NODE(J)
      DO 40 I=1,3
 40   F(I,N)=F(I,N)-P*B(J,I)
      RETURN
      END
```

```
      SUBROUTINE AHGHEX(NDF,V,F,NODE,ELEMP,E)
      DIMENSION V(NDF,1),F(NDF,1),NODE(8),ELEMP(3,4),E(3)
      DIMENSION GB(8,4),GS(8,4)
      COMMON /LOCAL/ X(8,3),B(8,3),VOL,AHR
      COMMON /TIME/ T,DT,NSTEP,MSTEP
      DATA GB/ 1., 1.,-1.,-1.,-1.,-1., 1., 1.,
     1         1.,-1.,-1., 1.,-1., 1., 1.,-1.,
     2         1.,-1., 1.,-1., 1.,-1., 1.,-1.,
     3        -1., 1.,-1., 1., 1.,-1., 1.,-1./
C
C     ANTI-HOURGLASSING ROUTINE FOR HEXAHEDRON ELEMENT
C     D. P. FLANAGAN       7/14/80
C
C     DESCRIPTION:
C          ANTI-HOURGLASSING FORCES ARE APPLIED GIVEN THE B-MATRIX,
C     ELEMENT COORDINATES, AND STIFFNESS RATIO.  THE HOURGLASSING BASE
C     VECTOR IS GIVEN.  THE HOURGLASSING SHAPE VECTOR IS COMPUTED USING
C     ORTHOGANALITY CONDITIONS.
C
C     VARIABLES:
C     NAME       TYPE       DESCRIPTION
C
C     NDF        INTEGER    NUMBER OF DIMENSIONS (3)
C     V          REAL       GLOBAL VELOCITIES
C     F          REAL       GLOBAL FORCES
C     NODE       INTEGER    ELEMENT NODE NUMBERS
C     ELEMP      REAL       HOURGLASS RESISTANCES
C     E          REAL       ELASTIC CONSTANTS
C                                1) DILATION MODULUS
C                                2) SHEAR MODULUS
C                                3) DENSITY
C     GB         REAL       HOURGLASS BASE VECTORS
C     GS         REAL       HOURGLASS SHAPE VECTORS
C     X          REAL       ELEMENT COORDINATES
C     B          REAL       B-MATRIX
C     VOL        REAL       ELEMENT VOLUME
C     AHR        REAL       ANTI-HOURGLASS RATIO
C     DT         REAL       TIME INCREMENT
C     A          REAL       STIFFNESS COEFFICIENT
C
C
C     COMPUTE ARTIFICIAL STIFFNESS
C     COMPUTE SHAPE VECTORS
C
      A=0.
      DO 10 I=1,8
      DO 10 J=1,3
      A=A+B(I,J)*B(I,J)
      SO=B(I,J)/VOL
      DO 10 K=1,4
      GS(I,K)=GB(I,K)
      DO 10 L=1,8
 10   GS(I,K)=GS(I,K)-SO*X(L,J)*GB(L,K)
      A=DT*AHR*(E(1)+E(2)+E(2))*A/(24.*VOL)
      DO 30 I=1,3
      DO 30 K=1,4
C
C     UPDATE HOURGLASS RESISTANCE
C
```

```
      S0=0.
      DO 20 J=1,8
   20 S0=S0+GS(J,K)*V(I,NODE(J))
      S0=ELEMP(I,K)+A*S0
      ELEMP(I,K)=S0
C
C     APPLY ANTI-HOURGLASSING FORCES
C
      DO 30 J=1,8
   30 F(I,NODE(J))=F(I,NODE(J))+S0*GS(J,K)
      RETURN
      END
```

```
      SUBROUTINE FHEX(NDF,XX,V,F,NODE,STRS,E)
      DIMENSION XX(NDF,1),V(NDF,1),F(NDF,1),NODE(4),STRS(3),E(4)
      DIMENSION S(3),G(2,2)
      COMMON /LOCAL/ X(4,2),B(4,2),AREA,AHR
      COMMON /TIME/ T,DT,NSTEP,MSTEP
C
C     INTERNAL FORCE ROUTINE FOR QUADRILATERAL (WITH HOOKE'S LAW)
C     D. P. FLANAGAN       6/9/80
C
C     DESCRIPTION:
C          THE INTERNAL FORCES FOR A QUADRILATERAL ARE CALCULATED FROM
C     THE ELEMENT MEAN STRESS TENSOR AND B-MATRIX.  THE B-MATRIX IS
C     DEFINED IN SUBROUTINE BQUAD.  THE STESS RATE IS COMPUTED FROM THE
C     MEAN VELOCITY GRADIENT AND LAME CONSTANTS.
C          THIS ROUTINE COUPLES WITH IHEX.
C
C     VARIABLES:
C     NAME       TYPE       DESCRIPTION
C
C     NDF        INTEGER    NUMBER OF DEGREES OF FREEDOM (2)
C     XX         REAL       GLOBAL COORDINATES
C     V          REAL       GLOBAL VELOCITIES
C     F          REAL       GLOBAL FORCES
C     NODE       INTEGER    ELEMENT NODE NUMBERS
C     STRS       REAL       ELEMENT STRESSES
C     E          REAL       ELASTIC CONSTANTS
C                                1) DILATION MODULUS
C                                2) SHEAR MODULUS
C                                3) DENSITY
C                                4) THICKNESS
C     X          REAL       ELEMENT COORDINATES
C     B          REAL       B-MATRIX
C     AREA       REAL       ELEMENT AREA
C     S          REAL       STRESS RATES
C     G          REAL       VELOCITY GRADIENT - STRESS TENSOR
C
C
C     EXTRACT ELEMENT COORDINATES
C
      DO 10 J=1,4
      N=NODE(J)
      DO 10 I=1,2
   10 X(J,I)=XX(I,N)
C
C     FIND B-MATRIX
C
      CALL BQUAD
C
C     COMPUTE VELOCITY GRADIENT
C
      DO 40 J=1,2
      DO 40 I=1,2
      G0=0.
      DO 30 K=1,4
   30 G0=G0+B(K,J)*V(I,NODE(K))
   40 G(I,J)=G0/AREA
C
C     COMPUTE STRESS RATES
C
      S0=E(1)*(G(1,1)+G(2,2))
      G0=G(1,2)-G(2,1)
      S(1)=S0+2.*E(2)*G(1,1)-G0*STRS(3)
      S(2)=S0+2.*E(2)*G(2,2)+G0*STRS(3)
      S(3)=E(2)*(G(1,2)+G(2,1))+G0*(STRS(2)-STRS(1))/2.
C
C     UPDATE STRESSES
C
```

```
      STRS(1)=STRS(1)+S(1)*DT
      G(1,1)=STRS(1)*E(4)
      STRS(2)=STRS(2)+S(2)*DT
      G(2,2)=STRS(2)*E(4)
      STRS(3)=STRS(3)+S(3)*DT
      G(2,1)=G(1,2)=STRS(3)*E(4)
C
C     ADD ELEMENT FORCES TO GLOBAL ARRAY
C
      DO 60 J=1,4
      N=NODE(J)
      DO 60 I=1,2
      DO 60 K=1,2
   60 F(I,N)=F(I,N)+G(I,K)*B(J,K)
      RETURN
      END

      SUBROUTINE AHGHEX(NDF,V,F,NODE,ELEMP,E)
      DIMENSION V(NDF,1),F(NDF,1),NODE(1),ELEMP(2),E(4)
      DIMENSION GB(4),GS(4)
      COMMON /LOCAL/ X(4,2),B(4,2),AREA,AHR
      DATA GB/ 1.,-1., 1.,-1./
C
C     ANTI-HOURGLASSING ROUTINE FOR QUADRILATERAL ELEMENT
C     D. P. FLANAGAN       6/9/80
C
C     DESCRIPTION:
C          ANTI-HOURGLASSING FORCES ARE APPLIED GIVEN THE B-MATRIX,
C     ELEMENT COORDINATES, AND DAMPING RATIO.  THE HOURGLASSING BASE
C     VECTOR IS GIVEN.  THE HOURGLASSING SHAPE VECTOR IS COMPUTED USING
C     ORTHOGANALITY CONDITIONS.
C
C     VARIABLES:
C     NAME      TYPE       DESCRIPTION
C
C     NDF       INTEGER    NUMBER OF DIMENSIONS (2)
C     V         REAL       GLOBAL VELOCITIES
C     F         REAL       GLOBAL FORCES
C     NODE      INTEGER    ELEMENT NODE NUMBERS
C     ELEMP     REAL       HOURGLASS RESISTANCES
C     E         REAL       ELASTIC CONSTANTS
C                               1) DILATION MODULUS
C                               2) SHEAR MODULUS
C                               3) DENSITY
C                               4) THICKNESS
C     GB        REAL       HOURGLASS BASE VECTORS
C     GS        REAL       HOURGLASS SHAPE VECTORS
C     X         REAL       ELEMENT COORDINATES
C     B         REAL       B-MATRIX
C     AREA      REAL       ELEMENT AREA
C     AHR       REAL       ANTI-HOURGLASS RATIO
C     A         REAL       DAMPING COEFFICIENT
C
C
C     COMPUTE ARTIFICIAL DAMPING
C     COMPUTE SHAPE VECTOR
C
      A=0.
      DO 10 I=1,4
      GS(I)=GB(I)
      DO 10 J=1,2
      A=A+B(I,J)*B(I,J)
      SO=B(I,J)/AREA
      DO 10 K=1,4
   10 GS(I)=GS(I)-SO*X(K,J)*GB(K)
      A=AHR*E(4)*SQRT(E(3)*(E(1)+E(2)+E(2))*A/8.)
      DO 30 I=1,2
C
C     UPDATE HOURGLASS RESISTANCE
C
      SO=0.
      DO 20 J=1,4
   20 SO=SO+GS(J)*V(I,NODE(J))
      SO=A*SO
      ELEMP(I)=SO
C
C     APPLY ANTI-HOURGLASSING FORCES
C
      DO 30 J=1,4
   30 F(I,NODE(J))=F(I,NODE(J))+SO*GS(J)
      RETURN
      END
```

```
      SUBROUTINE AHGHEX(NDF,V,F,NODE,ELEMP,E)
      DIMENSION V(NDF,1),F(NDF,1),NODE(1),ELEMP(2),E(4)
      DIMENSION GB(4),GS(4)
      COMMON /LOCAL/ X(4,2),B(4,2),AREA,AHR
      COMMON /TIME/ T,DT,NSTEP,MSTEP
      DATA GB/ 1.,-1., 1.,-1./
C
C     ANTI-HOURGLASSING ROUTINE FOR QUADRILATERAL ELEMENT
C     D. P. FLANAGAN        6/9/80
C
C     DESCRIPTION:
C          ANTI-HOURGLASSING FORCES ARE APPLIED GIVEN THE B-MATRIX,
C     ELEMENT COORDINATES, AND STIFFNESS RATIO.  THE HOURGLASSING BASE
C     VECTOR IS GIVEN.  THE HOURGLASSING SHAPE VECTOR IS COMPUTED USING
C     ORTHOGANALITY CONDITIONS.
C
C     VARIABLES:
C     NAME      TYPE       DESCRIPTION
C
C     NDF       INTEGER    NUMBER OF DIMENSIONS (2)
C     V         REAL       GLOBAL VELOCITIES
C     F         REAL       GLOBAL FORCES
C     NODE      INTEGER    ELEMENT NODE NUMBERS
C     ELEMP     REAL       HOURGLASS RESISTANCES
C     E         REAL       ELASTIC CONSTANTS
C                                1) DILATION MODULUS
C                                2) SHEAR MODULUS
C                                3) DENSITY
C                                4) THICKNESS
C     GB        REAL       HOURGLASS BASE VECTORS
C     GS        REAL       HOURGLASS SHAPE VECTORS
C     X         REAL       ELEMENT COORDINATES
C     B         REAL       B-MATRIX
C     AREA      REAL       ELEMENT AREA
C     AHR       REAL       ANTI-HOURGLASS RATIO
C     DT        REAL       TIME INCREMENT
C     A         REAL       STIFFNESS COEFFICIENT
C
C
C     COMPUTE ARTIFICIAL STIFFNESS
C     COMPUTE SHAPE VECTOR
C
      A=0.
      DO 10 I=1,4
      GS(I)=GB(I)
      DO 10 J=1,2
      A=A+B(I,J)*B(I,J)
      SO=B(I,J)/AREA
      DO 10 K=1,4
   10 GS(I)=GS(I)-SO*X(K,J)*GB(K)
      A=DT*AHR*(E(1)+E(2)+E(2))*E(4)*A/(8.*AREA)
      DO 30 I=1,2
C
C     UPDATE HOURGLASS RESISTANCE
C
      SO=0.
      DO 20 J=1,4
   20 SO=SO+GS(J)*V(I,NODE(J))
      SO=ELEMP(I)+A*SO
      ELEMP(I)=SO
C
C     APPLY ANTI-HOURGLASSING FORCES
C
      DO 30 J=1,4
   30 F(I,NODE(J))=F(I,NODE(J))+SO*GS(J)
      RETURN
      END
```

REFERENCES

1. D. S. Malkus and T. J. R. Hughes, 'Mixed finite element methods—reduced and selective integration techniques: a unification of concepts', *Comp. Meth. Appl. Mech. Engng*, **15**, 63–81 (1978).
2. B. Irons and S. Ahmad, *Techniques of Finite Elements*, Ellis Horwood, Chichester, England, 1980.
3. S. W. Key, Z. E. Beisinger and R. D. Krieg, 'HONDO II—a finite element computer program for the large deformation dynamic response of axisymmetric solids', Sandia Laboratories, Albuquerque, Oct. 1978.
4. G. Maenchen and S. Sack, 'The TENSOR Code', in *Methods in Computational Physics*, vol. 3 (Ed. B. Alder, *et al*), Academic Press, 1964, pp. 181–210.
5. A. G. Petschek and M. E. Hanson, 'Difference equations for two-dimensional elastic flow', *J. Comp. Phys.*, **3**, 307–321 (1968).

6. T. B. Belytschko, 'Finite element approach to hydrodynamics and mesh stabilization', in *Computation Methods in Nonlinear Mechanics* (Ed. J. T. Oden *et al*), The Texas Institute for Computational Mechanics, 1974.
7. M. L. Wilkins, R. E. Blum, E. Cronshagen and P. Grantham, 'A method for computer simulation of problems in solid mechanics and gas dynamics in three dimensions and time', Lawrence Livermore Laboratory, *Report UCRL-51574*, revision 1, May 1975.
8. T. B. Belytschko and J. M. Kennedy, 'Computer models for subassembly simulation', *Nucl. Engng Des.* **49**, 17–38 (1978).
9. S. W. Key, 'A finite element procedure for the large deformation dynamic response of axisymmetric solids', *Comp. Meth. Appl. Mech. Engng*, **4**, 195–218 (1974).
10. D. Kosloff and G. A. Frazier, 'Treatment of hourglass patterns in low order finite element codes', *Int. J. num. Anal. Meth. Geomech.* **2**, 57–72 (1978).
11. E. L. Wilson, R. L. Taylor, W. P. Doherty and J. Ghaboussi, 'Incompatible displacement models', in *Numerical and Computer Methods in Structural Mechanics*, (Ed. S. J. Fenves *et al*), Academic Press, New York, 1973, pp. 43–57.
12. O. C. Zienkiewicz, *The Finite Element Method in Engineering Science*, McGraw-Hill, London, 1971.
13. D. P. Flanagan and T. B. Belytschko, 'Eigenvalue bounds for uniform strain modes of the hexahedron and quadrilateral finite elements', in preparation.